Godunov-Type Solutions with Discrete Gas Cavity Model for Transient Cavitating Pipe Flow

Ling Zhou[1]; Huan Wang[2]; Anton Bergant[3]; Arris S. Tijsseling[4]; Deyou Liu[5]; and Su Guo[6]

Abstract: To simulate transient cavitating pipe flow, the discrete gas cavity model (DGCM) is combined with first-order and second-order finite-volume method (FVM) Godunov-type schemes. The earlier discrete vapor cavity model (DVCM) and DGCM based on the method of characteristics (MOC) are known to produce unrealistic pressure spikes. The new FVM-DGCM extends the previously developed FVM-DVCM through the introduction of a very small amount of free gas at the middle of each computation cell. Importantly, a pressure adjustment procedure is proposed to establish the relation between the cavity and the halves of the reach. Predictions of FVM-DGCM are compared with those of FVM-DVCM and MOC-DGCM and with experimental data. Results show that the proposed model reproduces the experimental pressure histories considerably better than the other two models. In particular, it produces fewer spikes, but—as in the old models—the first pressure peak due to cavity collapse is predicted much better than the subsequent peaks. The second-order FVM-DGCM is found to be accurate and robust, even for Courant numbers significantly less than 1. **DOI: 10.1061/(ASCE)HY.1943-7900.0001463.**

Author keywords: Pipe flow; Vaporous cavitation; Discrete gas cavity model; Finite volume method; Godunov-type scheme.

Introduction

Hydraulic transient events involving cavitation occur in pipelines whenever the pressure decreases to the vapor pressure of the liquid. The result is referred to as vaporous cavitation or liquid-column separation, and its occurrence has a significant impact on the subsequent transient response of the system. The extremely high pressures generated by cavity collapse may cause damage to and failures of pipe systems (Wylie et al. 1993; Bergant et al. 2006; Adamkowski and Lewandowski 2015).

Transients of this type have been investigated both numerically and experimentally. One of the widely used models for simulating cavitation in transient events is the discrete vapor cavity model (DVCM) combined with the method of characteristics (MOC), which covers the essential characteristics of transient cavitation (Wylie et al. 1993; Simpson and Bergant 1994). The major drawback of the classic MOC-DVCM is that the solution may generate unrealistic pressure spikes due to multicavity collapse when a relatively fine mesh is used (Bergant and Simpson 1999). In an effort to improve the performance of the MOC-DVCM, a small amount of noncondensable free gas is introduced into the standard DVCM to provide additional damping, and this addition is known as the discrete gas cavity model (DGCM) (Provoost and Wylie 1982; Wylie 1984; Vasconcelos and Marwell 2011; Malekpour and Karney 2014). The MOC-DGCM results obtained with a very low gas void fraction (order of 10^{-7} recommended at standard atmospheric conditions) show better agreement with experimental data than do the results of MOC-DVCM. However, the MOC-DVCM and the MOC-DGCM are usually poor in the prediction of the timing of repeated cavity formation and collapse (Bergant et al. 2006). The inclusion of unsteady skin friction into the DGCM may improve the numerical results significantly (Bergant et al. 2005). Guinot (2000) and Zhao and Ghidaoui (2004) introduced first-order and second-order explicit finite-volume method (FVM) Godunov-type schemes for water-hammer problems not involving vaporous cavitation. The latter demonstrated that the first-order Godunov scheme and the MOC scheme with space-line interpolation give identical results, and both cause strong numerical dissipation when the Courant number is less than 1.

The authors recently developed new methods to model vaporous cavitation in pipeline systems more accurately. Wang et al. (2016) developed a two-dimensional (2D) computational fluid dynamics (CFD) method which effectively calculates the pressure variations with the possibility of visualizing the underlying physical processes. Zhou et al. (2017) introduced a second-order explicit finite-volume method based on Godunov-type schemes to realize the solution of the classic DVCM. Although satisfactory results were obtained, FVM-DVCM in some cases still produced some oscillations near the pressure jumps, and therefore FVM needs further improvement regarding the simulation of vaporous cavitation.

This work proposes an approach combining the popular DGCM and FVM Godunov-type schemes to model the transient pressures associated with vaporous cavitation in pipelines. Compared with

[1]Professor, College of Water Conservancy and Hydropower Engineering, Hohai Univ., 1 Xikang Rd., Nanjing 210098, China (corresponding author). E-mail: zlhhu@163.com

[2]Ph.D. Candidate, College of Water Conservancy and Hydropower Engineering, Hohai Univ., 1 Xikang Rd., Nanjing 210098, China. E-mail: wanghuan0527@163.com

[3]Head, Dept. of Applied Research and Computations, Litostroj Power d.o.o., Litostrojska 50, 1000 Ljubljana, Slovenia. E-mail: anton.bergant@litostrojpower.eu

[4]Assistant Professor, Dept. of Mathematics and Computer Science, Eindhoven Univ. of Technology, P.O. Box 513, 5600 MB, Eindhoven, Netherlands. E-mail: a.s.tijsseling@tue.nl

[5]Professor, College of Water Conservancy and Hydropower Engineering, Hohai Univ., 1 Xikang Rd., Nanjing 210098, China. E-mail: Liudyhhuc@163.com

[6]Senior Experimentalist, College of Energy and Electrical Engineering, Hohai Univ., 1 Xikang Rd., Nanjing 210098, China. E-mail: guosu81@126.com

Note. This manuscript was submitted on February 15, 2017; approved on November 22, 2017; published online on March 15, 2018. Discussion period open until August 15, 2018; separate discussions must be submitted for individual papers. This paper is part of the ***Journal of Hydraulic Engineering***, © ASCE, ISSN 0733-9429.

the previous FVM-DVCM, the proposed FVM-DGCM introduces a small amount of free gas in the middle of each pipe reach. Because of the fundamental differences between MOC and FVM schemes, the strategy of modeling the gas cavity in relation to its adjacent pipe reaches is in FVM significantly different from the approach in MOC-DGCM. The new model aims to better predict the pressure fluctuations and, in particular, to avoid the unrealistic pressure spikes that are often present in previous formulations.

This paper formulates the first-order and second-order FVM-DGCM and then validates them using published experimental data (Simpson 1986; Bergant and Simpson 1999). The effects of initial free gas fraction, grid number, pressure-adjustment coefficient, and Courant number are investigated. The popular MOC-DGCM with staggered grid (Wylie et al. 1993) and the second-order FVM-DVCM (Zhou et al. 2017) are used for comparison.

Governing Equations of Water Hammer with Discrete Gas Cavities

Some basic assumptions on modeling free gas in the MOC-DGCM are still necessary to develop the FVM-DGCM. Volumes of free gas are lumped at discrete computational sections. As the pressure changes, each isolated small volume of free gas expands and contracts isothermally (because the gas bubbles are relatively small and surrounded by liquid of assumed constant temperature). Pure liquid with constant wave speed is assumed to occupy the reaches that connect the gas cavities. The wave speed remains constant throughout the simulation. Liquid mass conservation is preserved at each gas volume by applying a local continuity relationship.

To realize the FVM solution including the DGCM, the following assumptions are essential: (1) free gas is lumped as a cavity at the middle of each reach; (2) to accommodate the gas cavity, each reach is divided into halves (two equal parts); (3) pressure and discharge in the two halves are calculated by FVM identical to the calculation of pure water hammer; and (4) the variation of each gas cavity volume is governed by the discharges in the adjacent half reaches.

Fig. 1 shows a section of pipeline with a gas volume concentrated at each computational section. The perfect gas law is used to determine the volume of each constant mass of free gas, which can be written as

$$M_g R_g T = p_g^* \alpha \quad \forall = p_0^* \alpha_0 \quad \forall \tag{1}$$

where T = absolute temperature; M_g = mass of gas; R_g = specific gas constant; $\forall$ = volume of a pipe reach; and α_0 = gas void fraction at standard (reference) absolute pressure, p_0^*. Note that $\alpha_0 = \forall_{g0}/\forall$, where $\forall_{g0}$ is initial volume of the lumped gas cavity.

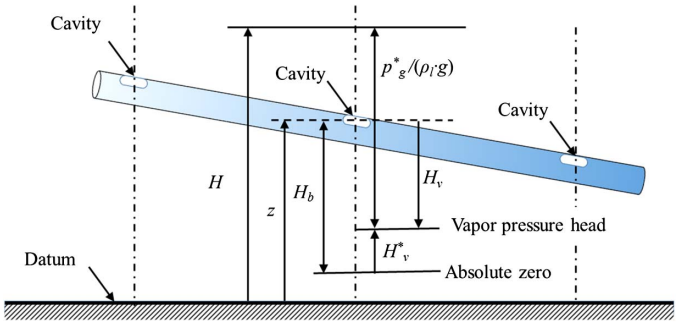

Fig. 1. Discrete free-gas cavities and piezometric heads in liquid pipeline

The hydraulic-grade line is conveniently used to deal with free gas in water, so the absolute pressure p_g^* of the free gas can be expressed (according to Fig. 1) as

$$p_g^* = \rho_l g(H - z - H_v) \tag{2}$$

where H = hydraulic-grade line, sometimes called piezometric head or head (Wylie et al. 1993); ρ_l = density of the liquid; g = gravitational acceleration; z = elevation of the pipeline; and H_v = gauge vapor pressure head, where $H_v = \{[(p_v^*)/(\rho_l g)] - H_b\}$ is absolute barometric pressure head and p_v^* = absolute vapor pressure.

The continuity equation for the gas volume is

$$\frac{d\forall_g}{dt} = Q - Q_u \tag{3}$$

where $\forall_g$ = volume of the discrete gas cavity; and Q and Q_u = flow rates downstream and upstream of the gas cavity, respectively.

The continuity and momentum equations for classic water hammer can be written in the form of a Riemann problem (Guinot 2000; Zhao and Ghidaoui 2004; Zhou et al. 2017)

$$\frac{\partial \mathbf{u}}{\partial t} + \frac{\partial \mathbf{f}(\mathbf{u})}{\partial x} = \mathbf{s}(\mathbf{u}), \qquad \mathbf{f}(\mathbf{u}) = \boldsymbol{A}\mathbf{u} \tag{4}$$

where $\mathbf{u} = \begin{pmatrix} H \\ V \end{pmatrix}$; $\boldsymbol{A} = \begin{pmatrix} 0 & a^2/g \\ g & 0 \end{pmatrix}$; $\mathbf{s}(\mathbf{u}) = \begin{pmatrix} 0 \\ -\frac{f|V|V}{2D} \end{pmatrix}$; distance x along the pipeline and time t are independent variables; V = average cross-sectional velocity; a = wave speed; f = Darcy–Weisbach friction factor; and D = pipe inner diameter.

Godunov-Type Schemes for Water Hammer

The pipeline is divided into N_s reaches with length $\Delta x'$ (which is equal to $2\Delta x$) and reach center index j. The discrete cavity is at the midpoint of the reach and each reach is divided into halves to accommodate standard application of FVM. Fig. 2 shows the grid system: the half grid length is Δx and the doubled grid number is $N = 2N_s$. As in DGCM, the grid is fixed with constant Δx during the entire transient process regardless of the size of the discrete cavity. The pressure and flow rate are determined from FVM Godunov-type solutions on the adjacent reaches, identical to the procedure applied in the pure water-hammer problem (Zhou et al. 2017).

The ith cell in the FVM is centered at node i and extends from $i - 1/2$ to $i + 1/2$. The flow variables (H and V) are defined at the cell centers i and represent their average values within each cell. Fluxes are calculated at the interfaces ($i - 1/2$ and $i + 1/2$)

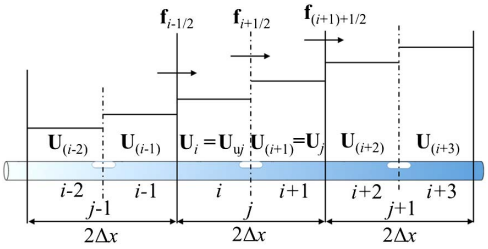

Grid length: $\Delta x = 0.5\Delta x'$, grid number: $N = 2N_s$, $i+1 = 2j$

Fig. 2. Discretization grids

between cells. For the ith cell, the integration of Eq. (4) with respect to x between control surfaces $i-1/2$ and $i+1/2$ yields

$$\mathbf{U}_i^{n+1} = \mathbf{U}_i^n - \frac{\Delta t}{\Delta x}(\mathbf{f}_{i+1/2}^n - \mathbf{f}_{i-1/2}^n) + \frac{\Delta t}{\Delta x}\int_{i-1/2}^{i+1/2} \mathbf{s}\,dx \quad (5)$$

where $\mathbf{U}_i$ = mean value of $\mathbf{u}$ in the interval $[i-1/2, i+1/2]$; and superscripts n and $n+1$ indicate the t and $t+\Delta t$ time levels, respectively. In Eq. (5), the value of $\mathbf{U}$ at new time step $n+1$ requires the computation of the numerical fluxes at the cell interfaces at previous time n and the integrated source term.

Computation of Flux Term

In the Godunov approach, the numerical flux is determined by solving a local Riemann problem at each cell interface (Guinot 2000). Applying Rankine–Hugoniot conditions $\Delta\mathbf{f} = \overline{A}\Delta\mathbf{u} = \overline{\lambda}_i\Delta\mathbf{u}$ across each wave front traveling at speed $\overline{\lambda}_i$ ($i = 1$, 2, and eigenvalues $\overline{\lambda_1} = -a$ and $\overline{\lambda_2} = a$), the fluxes at $i+1/2$ for all internal nodes and for $t \in [t^n, t^{n+1}]$ are as follows (Zhao and Ghidaoui 2004; Zhou et al. 2017):

$$\begin{aligned}\mathbf{f}_{i+1/2} &= \overline{\mathbf{A}}_{i+1/2}\boldsymbol{u}_{i+1/2} \\ &= \frac{1}{2}\overline{\mathbf{A}}_{i+1/2}\left[\begin{pmatrix} 1 & a/g \\ g/a & 1 \end{pmatrix}\mathbf{U}_L^n - \begin{pmatrix} -1 & a/g \\ g/a & -1 \end{pmatrix}\mathbf{U}_R^n\right]\end{aligned} \quad (6)$$

where $\overline{\mathbf{A}}_{i+1/2} = \mathbf{A}$ because the convective terms are neglected in the standard water-hammer equations; $\mathbf{U}_L^n$ = average value of $\mathbf{u}$ to the left of interface $i+1/2$ at time n; and $\mathbf{U}_R^n$ = average value of $\mathbf{u}$ to the right of interface $i+1/2$ at time n (Fig. 2).

Both $\mathbf{U}_L^n$ and $\mathbf{U}_R^n$ are estimated from a polynomial reconstruction the order of which determines the spatial accuracy of the numerical scheme. For Godunov's first-order accuracy method, a piecewise constant approximation is used, namely $\mathbf{U}_L^n = \mathbf{U}_i^n$ and $\mathbf{U}_R^n = \mathbf{U}_{i+1}^n$. To achieve second-order accuracy in space and time, this paper uses the monotonic upstream-centered scheme for conservation laws (MUSCL)-Hancock method. The MINMOD limiter is introduced to ensure that the results remain free of spurious oscillations. Toro (2009) gave details of the MUSCL-Hancock method.

This paper uses virtual cells I_{-1} and I_0 adjacent to I_1, and virtual cells I_{N+1} and I_{N+2} adjacent to I_N, to achieve the direct solution of the Riemann problem for the boundary unknowns $\mathbf{U}_1$ and $\mathbf{U}_N$. It is assumed that the flow information in the virtual cells is the same as at the boundaries, that is $\mathbf{U}_{-1}^{n+1} = \mathbf{U}_0^{n+1} = \mathbf{U}_{1/2}$ and $\mathbf{U}_{N+1}^{n+1} = \mathbf{U}_{N+2}^{n+1} = \mathbf{U}_{N+1/2}$, where $\mathbf{U}_{1/2}$ and $\mathbf{U}_{N+1/2}$ are obtained by coupling the Riemann invariant with a head-flow boundary relation at time n (Zhou et al. 2017).

Incorporation of Source Terms

Source terms $\mathbf{s}(\mathbf{u})$ and their spatial integration are introduced into the solution through time splitting and using a second-order Runge–Kutta discretization which results in the following explicit procedure.

First step (pure wave propagation)

$$\overline{\mathbf{U}}_i^{n+1} = \mathbf{U}_i^n - \frac{\Delta t}{\Delta x}(\mathbf{f}_{i+1/2}^n - \mathbf{f}_{i-1/2}^n) \quad (7)$$

Second step (update with source term at $\Delta t/2$)

$$\overline{\overline{\mathbf{U}}}_i^{n+1} = \overline{\mathbf{U}}_i^{n+1} + \frac{\Delta t}{2}\mathbf{s}(\overline{\mathbf{U}}_i^{n+1}) \quad (8)$$

Last step (reupdate with source term at Δt)

$$\mathbf{U}_i^{n+1} = \overline{\mathbf{U}}_i^{n+1} + \Delta t\mathbf{s}(\overline{\overline{\mathbf{U}}}_i^{n+1}) \quad (9)$$

The convective terms are neglected in the governing Eq. (4) in the proposed FVM-DGCM. Thus the Courant–Friedrichs–Lewy (CFL) criterion $C_r = a\Delta t/\Delta x \le 1$ is satisfied in advance (because a is constant) by taking Δt small enough for given Δx.

Crucial Strategies on Discrete Free-Gas Cavities

Simulation of discrete gas cavities is the key ingredient in the application of Riemann-based FV schemes in DGCM. Finite-volume methods can provide correct jump relations for traveling discontinuities (Zhao and Ghidaoui 2004; Toro 2009). The numerical discontinuity appears at the interface between ith and $(i+1)$th cells, which is essentially different from the continuity feature at the computed node in the MOC scheme. Precisely because of this essential distinction between the two schemes, the solution process in FVM-DGCM is significantly different from that in MOC-DGCM.

In MOC-DGCM, the hydraulic-grade line and volume of the gas cavity [$H_{g(j)}^{n+1}$ and $\forall_{g(j)}^{n+1}$], and the piezometric head and the flow rate at the upstream and downstream ends of the gas cavity (H_{uj}^{n+1}, Q_{uj}^{n+1}, H_j^{n+1}, and Q_j^{n+1}) are obtained at each computational section via a quadratic equation that combines the ideal gas law, two MOC compatibility equations, and the continuity of the gas volume (Wylie et al. 1993), noting that $H_{g(j)}^{n+1} = H_{uj}^{n+1} = H_j^{n+1}$. However, the piezometric head and discharge in the cells in FVM are directly determined from the exact solution of the Riemann problem (Zhao and Ghidaoui 2004; Toro 2009; Zhou et al. 2017), from which it is impossible to form a quadratic equation as in the MOC, that is, the variables [$H_{g(j)}^{n+1}$, $\forall_{g(j)}^{n+1}$, H_{uj}^{n+1}, Q_{uj}^{n+1}, H_j^{n+1}, and Q_j^{n+1}] cannot simultaneously be solved. In the proposed FVM-DGCM at each time step, the first step is to obtain the piezometric head and discharge in the two halves in which each reach is divided (H_i^{n+1}, Q_i^{n+1}, H_{i+1}^{n+1}, and Q_{i+1}^{n+1}, which are equal to H_{uj}^{n+1}, Q_{uj}^{n+1}, H_j^{n+1}, and Q_j^{n+1}, respectively) by the Godunov scheme, where the head values are not limited by the condition of $H_{uj}^{n+1} = H_j^{n+1}$ (unlike in MOC-DGCM). Then, depending on whether or not the pressure H_{uj}^{n+1} or H_j^{n+1} decreases to the vapor pressure of the liquid, two different methods are proposed to calculate the head and volume of the discrete gas cavity.

Method I: Pressure above Vapor Pressure

The piezometric head and discharge in the two cells (i and $i+1$) defining the jth reach in Fig. 2 are calculated by FVM independent of the gas cavity volume. When the pressures in both halves of the reach are higher than the vapor pressure, $H_{g(j)}^{n+1}$ is set equal to the arithmetic average value of the head at both halves

$$H_{g(j)}^{n+1} = (H_{uj}^{n+1} + H_j^{n+1})/2 \quad (10)$$

Substitution of Eq. (10) into Eq. (2) gives the volume of the gas cavity

$$\forall_{g(j)}^{n+1} = p_0^*\alpha_0\forall/[\rho_l g(H_{g(j)}^{n+1} - z(j) - H_v)] \quad (11)$$

Because the existence of the discrete gas cavity affects the adjacent halves, the heads in the halves of the reach must be adjusted

J. Hydraul. Eng., 2018, 144(5): 04018017

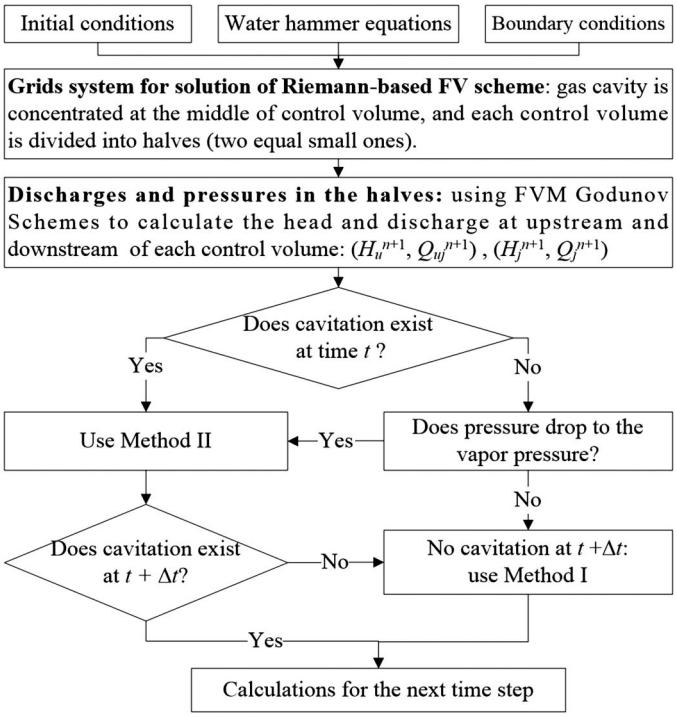

Fig. 3. Flowchart for FVM-DGCM

according to the gas pressure. The linear relation between the head in the gas cavity and the adjacent halves of the reach is proposed as

$$H_{uj}^{n+1} = C_{-ap} H_{uj}^{n+1} + (1 - C_{-ap}) H_{g(j)}^{n+1} \tag{12}$$

$$H_{j}^{n+1} = C_{-ap} H_{j}^{n+1} + (1 - C_{-ap}) H_{g(j)}^{n+1} \tag{13}$$

where C_{-ap} = adjustment coefficient (or a relaxation factor) ranging from 0 to 1; $C_{-ap} = 0$ means that $H_{g(j)}^{n+1} = H_{uj}^{n+1} = H_j^{n+1}$, whereas for $C_{-ap} = 1$ the influence of the gas cavity is entirely ignored. Note that for $C_{-ap} = 1$ the method is the same as FVM-DVCM. The value of C_{-ap} has a significant influence on the numerical damping of transient heads, which is discussed subsequently.

Method II: Pressure at or below Vapor Pressure

Once any pressure in the two halves of the reach is at or below the liquid's vapor pressure, the gas volume is determined from the continuity Eq. (3). The volume change $\Delta \forall_{g(j)}$ in terms of the difference in discharges ΔQ_j at the upstream and downstream side of the cavity is

$$\Delta \forall_{g(j)} = \int_t^{t+\Delta t} \Delta Q_j dt = \int_t^{t+\Delta t} (Q_j - Q_{uj}) dt \tag{14}$$

The gas cavity volume at $t = t + \Delta t$ is computed implicitly by

$$\forall_{g(j)}^{n+1} = \forall_{g(j)}^{n} + (Q_j^{n+1} - Q_{uj}^{n+1}) \Delta t \tag{15}$$

where Q_{uj}^{n+1} and $Q_j^{n+1} = Q_i^{n+1}$ and Q_{i+1}^{n+1}, respectively (Fig. 2).

Substitution of Eq. (15) into Eqs. (1) and (2) gives the relation

$$H_{g(j)}^{n+1} = \frac{p_0^* \alpha_0 \forall}{\rho_l g \forall_{g(j)}^{n+1}} + z(j) + H_v \tag{16}$$

Both H_{uj}^{n+1} and H_j^{n+1} are set as the head at the gas cavity, namely

$$H_{uj}^{n+1} = H_j^{n+1} = H_{g(j)}^{n+1} \tag{17}$$

Fig. 3 illustrates the flow diagram of the FVM-DGCM for water column separation (WCS).

Results and Discussions

To evaluate the accuracy of the first-order and second-order FVM-DGCM in simulating vaporous cavitation in water pipelines, the calculated pressure histories were compared with experimental data. The influences of initial free gas void fraction α_0, pressure adjustment coefficient C_{-ap}, Courant number C_r, and grid number N_s were investigated. Moreover, the previous FVM-DVCM (Zhou et al. 2017) and the popular MOC-DGCM with staggered grid (Wylie et al. 1993) were used for comparison.

Simpson (1986) designed and constructed an experimental apparatus to investigate column separation events in pipelines. The apparatus comprised an upward-sloping copper pipe connecting two pressurized tanks, and a downstream valve. The pipe inlet location was lower than the outlet, and the pipe slope was 1:36. In the experiments, an initial steady-state flow was established toward the upper tank. The ball valve was then closed suddenly to create transient flow with vaporous cavitation. Two experimental cases (Case 1 and Case 2) that generated vaporous cavitation upstream of the valve were selected to assess the accuracy of the mathematical models; Table 1 summarizes the relevant experimental conditions and input data. Another physical model used in this study was a similar experimental apparatus from Bergant and Simpson (1999). The pipe was 37.2 m long with an upward slope of 3.2° (i.e., the pipe inlet location was lower than the outlet). Table 1 lists the conditions for this Case 3. Moreover, pure water hammer in a theoretical frictionless horizontal pipe system is also presented as a basic reference solution (Case 0 in Table 1).

Comparisons with Experimental Data and Numerical Tests

Water hammer with and without cavitation was simulated by the proposed FVM-DGCM using $N_s = 32$ or 256 computational reaches and compared with theoretical and experimental data for the four cases in Table 1.

Table 1. Conditions for the Experimental and Theoretical Cases

Case number	V_0 (m/s)	H_r (m)	T_c (s)	D (mm)	L (m)	a (m/s)	Data source
0	0.16	23.41	0.0	19.05	36.0	1,280	Theoretical (frictionless and horizontal pipe)
1	0.332	23.41	0.022	19.05	36.0	1,280	Simpson (1986)
2	1.125	21.74	0.024	19.05	36.0	1,280	Simpson (1986)
3	0.30	22.0	0.009	22.10	37.2	1,319	Bergant and Simpson (1999)

J. Hydraul. Eng., 2018, 144(5): 04018017

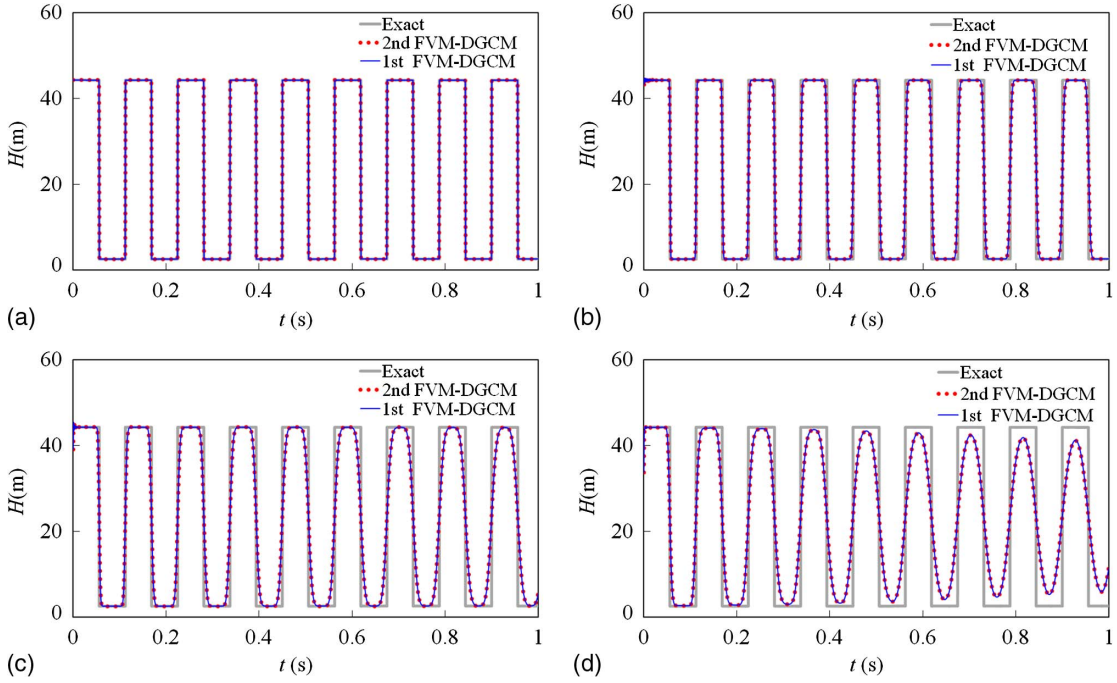

Fig. 4. Pure water hammer of Case 0 calculated by FVM-DGCM with different C_{-ap} ($N_s = 32$, $C_r = 1$): (a) $C_{-ap} = 1$; (b) $C_{-ap} = 0.9$; (c) $C_{-ap} = 0.5$; (d) $C_{-ap} = 0$

Influence of C_{-ap} in Proposed FVM-DGCM

The key coefficient C_{-ap} ranging from 0 to 1 was introduced in the solution of the proposed FVM-DGCM. The theoretical Case 0 in Table 1 was used to validate the proposed FVM-DGCM in the absence of cavitation and to analyze the effect of the pressure adjustment coefficient C_{-ap} on the numerical dissipation. Fig. 4 compares results calculated by the first-order and second-order FVM-DGCM with C_{-ap} = {0, 0.5, 0.9, and 1} together with the exact solution. The initial free gas volume fraction $\alpha_0 = 10^{-7}$ as recommended in the classic MOC-DGCM (Wylie et al. 1993), the Courant number $C_r = 1.0$, and the number of reaches $N_s = 32$.

The results with $C_{-ap} = 1.0$ in Fig. 4(a) were completely consistent with the exact data, proving that the proposed FVM approach can accurately simulate the case of pure water hammer. That is because with $C_{-ap} = 1.0$, there was no adjustment of the heads [Eqs. (12) and (13)] and the influence of the discrete gas cavities was absent. Figs. 4(b–d) show that when $C_{-ap} < 1.0$, the pressure heads exhibited numerical dissipation, which became more serious as C_{-ap} decreased. Taking $C_{-ap} = 0$ caused the largest artificial damping [Fig. 4(d)] because the heads in the cells adjacent to each cavity were simply taken equal to their arithmetic averages. The proposed FVM-DGCM advises values of C_{-ap} from 0.5 to 1 because lower values give too much numerical damping.

Influence of α_0 in Proposed FVM-DGCM

The effect of the initial gas void fraction in the classic MOC-DGCM has been investigated thoroughly (Wylie 1984; Wylie et al. 1993; Liou 2000). It has been demonstrated that the MOC-DGCM with $\alpha_0 \leq 10^{-7}$ at standard conditions can be used to simulate transient flow with vaporous cavitation because there is a negligible change in wave speed a due to the presence of the small amount of free gas, even at low pressures. Fig. 5 compares results calculated by the second-order FVM-DGCM with $\alpha_0 = \{10^{-7}, 10^{-8}, 10^{-10}\}$ with the experimental data for Case 1 in Table 1. In the simulations, $C_{-ap} = 0.9$, $C_r = 1.0$, and $N_s = 32$.

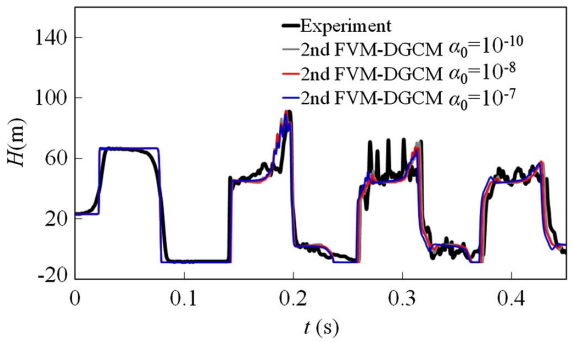

Fig. 5. Effects of α_0 in second-order FVM-DGCM on transient pressures at end valve in Case 1

Fig. 5 reveals that when $\alpha_0 \leq 10^{-7}$, the pressure heads calculated for an event with vaporous cavitation were basically identical. Therefore, $\alpha_0 = 10^{-7}$ is taken herein as a standard value.

Validation of Second-Order FVM-DGCM

Two distinct experimental runs involving a small and a large vapor cavity at the downstream end of a simple reservoir–pipe–valve system were selected to assess the ability of the numerical models to simulate vaporous cavitation. For the small vapor cavity (Cases 1 and 3 in Table 1), a narrow short-duration pressure pulse was generated, which was higher than the water-hammer pressure before cavitation occurred. This short-duration pressure pulse resulted from the superposition of waves originating from the reservoir, from the cavity collapse, and from the closed valve. For the large vapor cavity (Case 2 in Table 1), there was no such distinct short-duration pressure pulse. In the simulations, $\alpha_0 = 10^{-7}$ at standard conditions, C_{-ap} = {1.0, 0.9, 0.8 and 0.5}, the Courant number $C_r = 1.0$, and $N_s = \{32,256\}$.

Fig. 6 shows the calculated and experimental pressure-head histories in the case with a relatively small vapor cavity at the valve

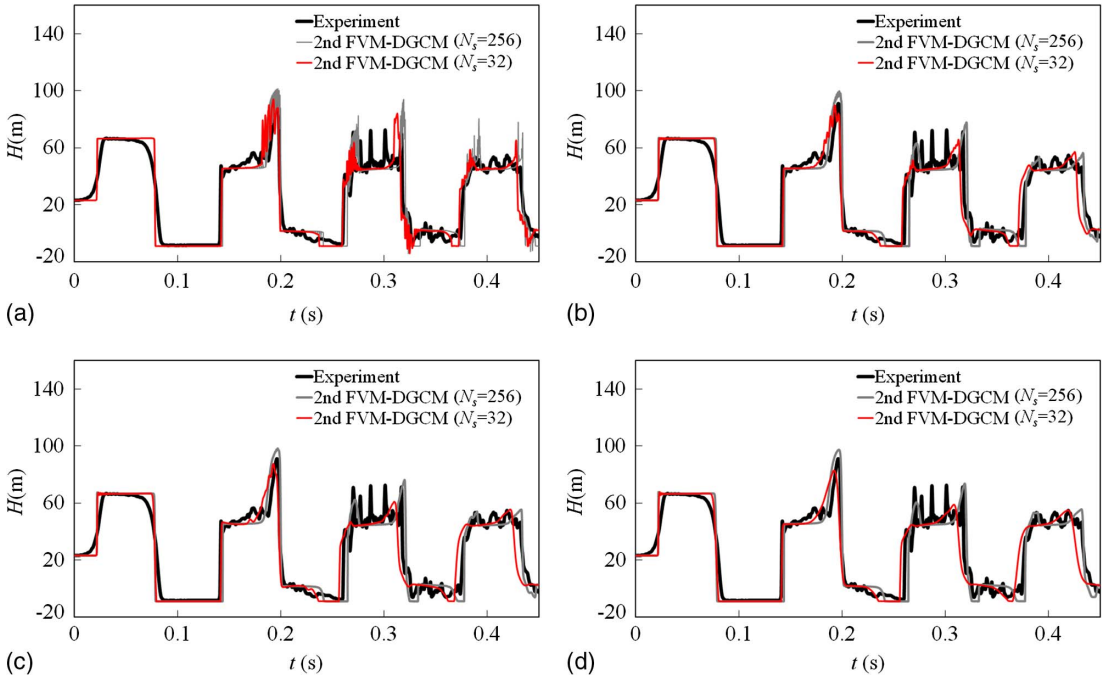

Fig. 6. Transient pressures in Case 1 calculated by second-order FVM-DGCM with different C_{-ap}: (a) $C_{-ap} = 1.0$; (b) $C_{-ap} = 0.9$; (c) $C_{-ap} = 0.8$; (d) $C_{-ap} = 0.5$

(Case 1 in Table 1). Both amplitude and timing of all simulated pressure heads displayed acceptable agreement with the experimental data. With $C_{-ap} = 1.0$, high-frequency pressure peaks (spikes) were superimposed on the bulk pressures [Fig. 6(a), $N_s =$ 32 or 256]. This effect intensified as the grid number increased. As the value of C_{-ap} decreased from 1 to 0.5, the spikes gradually dissipated. The coefficient C_{-ap} thus effectively controlled high-frequency pressure spikes in discrete cavity models. For $C_{-ap} =$ 0.5, the peak pressures were underestimated when the coarser grid was used [Fig. 6(d)]; $C_{-ap} = 0.9$ gave the best match between computed and measured results [Fig. 6(b)].

Fig. 7 shows that the proposed model with 32 reaches predicted very well the transient pressure-heads for the case with a large vapor cavity at the valve (Case 2 in Table 1). Fig. 8 compares the calculated pressure heads against the experimental records for Case 3. All calculations with C_{-ap} = {1.0 and 0.9} gave a good prediction with regard to the timing and amplitude of the bulk pressures. Using $C_{-ap} = 1.0$ resulted in unrealistic spikes, which were significantly damped once the value of C_{-ap} was slightly less than 1.

Overall, the proposed second-order FVM-DGCM with $C_{-ap} =$ 0.9 is a robust method for the simulation of fluid transients with vaporous cavitation.

Comparison between First-Order and Second-Order FVM-DGCMs

The difference between the first-order and second-order FVM-DGCM is only the order of accuracy in time and space in the solution of the water-hammer equations. In order to assess the first-order FVM-DGCM against the second-order FVM-DGCM, Figs. 4 and 9 compare pure water hammer in the frictionless theoretical Case 0 (in Table 1) with the transients with vaporous cavitation in the experimental Case 1. In the simulations for Case 1 in Fig. 9, $\alpha_0 = 10^{-7}$, $N_s = 32$, $C_{-ap} = 0.9$, and Courant number C_r = {1.0, 0.5, and 0.1}.

Fig. 4 shows that for pure water hammer and $C_r = 1$, the plotted pressure heads overlapped for the first-order and second-order methods, independent of the values of C_{-ap} and N_s. For pure water

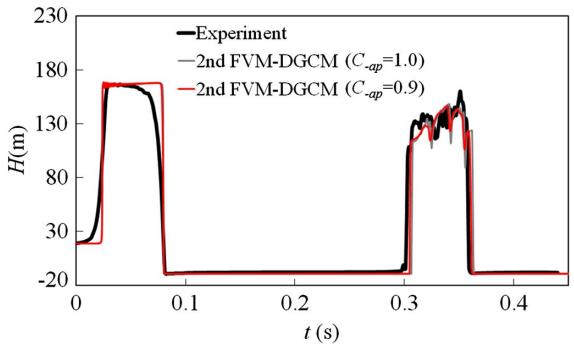

Fig. 7. Transient pressures in Case 2 calculated by second-order FVM-DGCM ($N_s = 32$)

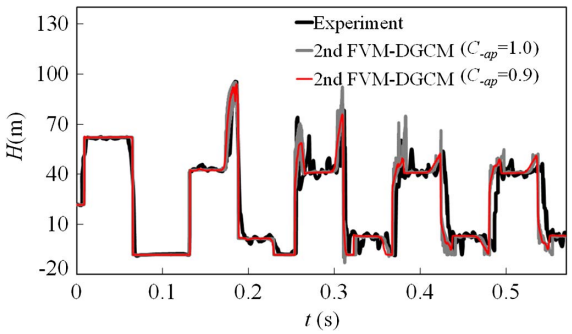

Fig. 8. Transient pressures in Case 3 calculated by second-order FVM-DGCM ($N_s = 256$)

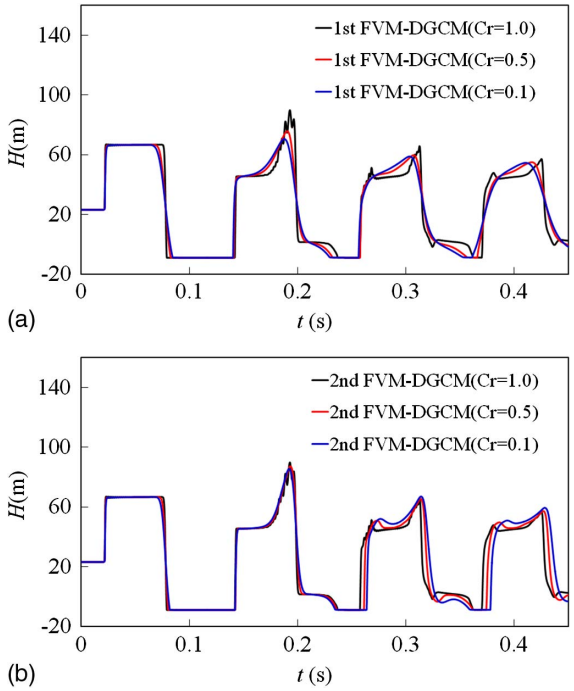

Fig. 9. Effect of Courant number in FVM-DGCM on transient pressure heads at valve in Case 1 with $C_{\_ap} = 0.9$: (a) first-order scheme; (b) second-order scheme

hammer, the proposed FVM-DGCM with $\alpha_0 = 10^{-7}$ and the model of Zhao and Ghidaoui (2004) produced consistent results because the same Godunov schemes were applied. Zhao and Ghidaoui (2004) demonstrated that in pure water-hammer simulations, the first-order FVM scheme causes significant numerical damping when $C_r < 1$, whereas the second-order scheme is more accurate for a Courant number less than 1.

When $C_r = 1$, the first-order and second-order FVM-DGCM produced practically identical results (Fig. 9). When $C_r < 1$, the first-order method exhibited larger numerical dissipation than the second-order method and significantly underestimated the maximum pressure [Fig. 9(a)]. Fig. 9(b) demonstrates that the second-order method produced accurate pressure-head histories.

The results indicate that the second-order method effectively simulated water-hammer problems and vaporous cavitation even when the Courant number was less than 1. The first-order FVM-DGCM can reach the same accuracy as the second-order FVM-DGCM only when $C_r = 1$.

Comparison with FVM-DVCM

The FVM-DGCM introduces a low initial gas void fraction $\alpha_0 \leq 10^{-7}$ into the FVM-DVCM scheme (Zhou et al. 2017). In the FVM-DVCM, the head and discharge are directly determined from the exact solution of the Riemann problem, and the vapor cavity volume is zero when the pressure is above the vapor pressure. Once the pressure falls to the vapor pressure, the pressures in the halves of the reach are set to the liquid's vapor pressure, and the vapor volume is determined by the discharges of the halves. Compared with the FVM-DVCM, the most important difference is that the heads in the halves of the reach are influenced by the gas cavity, unlike FVM-DVCM, in which the pressures are directly determined from the exact solution of the Riemann problem.

Fig. 10 depicts the transient pressure-head histories for Case 1 produced by the second-order FVM-DVCM (Zhou et al. 2017)

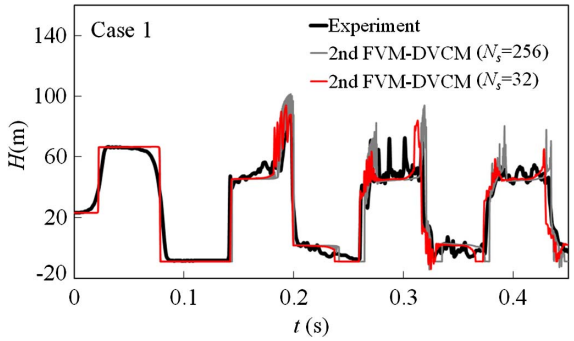

Fig. 10. Comparison of results from second-order FVM-DVCM against experimental data of Case 1

with $N_s = 32$ or 256. High-frequency spikes were a feature of the DVCM ($N_s = 32$) and these became more prominent as the grid number increased ($N_s = 256$). By definition, the second-order FVM-DGCM with $C_{\_ap} = 1$ produced identical results to those of the second-order FVM-DVCM [Figs. 6(a) and 10].

Comparison with MOC-DGCM

The common factor of FVM-DGCM and MOC-DGCM is that a small amount of noncondensable free gas is assumed to be concentrated at computational sections. However, the solution processes are different in the two models due to an essential distinction between FVM and MOC schemes, as detailed previously.

Fig. 11 presents transient pressure heads for Case 1 predicted by MOC-DGCM (Wylie et al. 1993) with $N_s = 32$ or 256. This method might produce unrealistic pressure spikes when finer grids are used. Fig. 11 also shows the different timing of the cavity collapse and superposition of the waves between the measured and computed results. The time discrepancies may be attributed to approximate modeling of column separation along the pipeline (distributed vaporous cavitation region, actual number, and position of intermediate cavities), the closure law of the ball valve being simply considered as a linear closure, the unsteady friction term being approximated as a steady-state friction term, and uncertainties in measurement (Simpson and Bergant 1994; Bergant and Simpson 1999). The results of FVM-DGCM with $C_{\_ap} = 0.9$ showed considerably better agreement with the experimental data (Fig. 6). Moreover, the MOC-DGCM is restricted to first-order accuracy, and it is difficult and complicated to realize second-order accuracy. As discussed previously and by Zhao and Ghidaoui (2004), the first-order accuracy in both MOC and FVM solutions

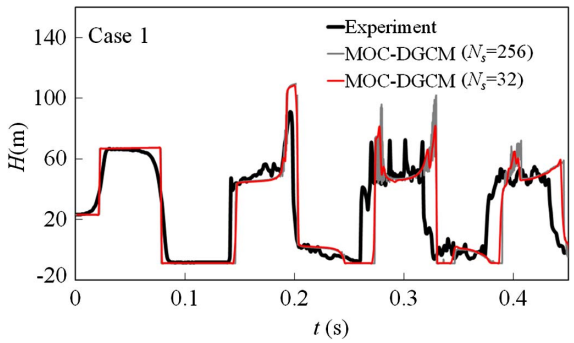

Fig. 11. Comparison of results from MOC-DGCM against measured data of Case 1

involves significant numerical dissipation once the Courant number is less than 1.

Compared with the classical MOC-DGCM, the second-order FVM-DGCM proposed in this paper is more suitable to simulate transient vaporous cavitation for Courant numbers less than or equal to 1, even when fine computational grids are used.

Conclusions

The discrete gas cavity model with MOC solution has been widely used to predict the dynamic behavior of vaporous cavitation in pipe systems. This paper proposed first-order and second-order FVM Godunov-type schemes for the DGCM to simulate water hammer with vaporous cavitation. Two methods were proposed to calculate the pressure and volume of discrete gas cavities depending on whether or not the pressure decreases to the vapor pressure of the liquid. A pressure adjustment coefficient C_{-ap} was introduced to establish the relation between the gas cavity and the halves of the reach. Results calculated by the FVM-DGCM were compared with published experimental data and with predictions by the classical MOC-DGCM and the FVM-DVCM. The main conclusions are

1. The coefficient C_{-ap} plays an important role in the realization of the FVM solution in the DGCM; it causes artificial damping due to pressure interpolation when $C_{-ap} < 1$.
2. For frictionless pure water-hammer problems, $C_{-ap} = 1$ provides exact results. For $C_{-ap} < 1$, the results exhibit artificial dissipation, which becomes the most severe when $C_{-ap} = 0$. The values of C_{-ap} in the range from 0.5 to 1 cause acceptable damping, which has little or no impact on the main pressure pulses.
3. For transient events with vaporous cavitation, $C_{-ap} = 1$ may produce unrealistic pressure peaks, especially when regions of distributed vaporization occur. When C_{-ap} is close to 0.5, the maximum pressures are likely to be underestimated, in particular when a sparse grid is applied. A value of C_{-ap} close to 0.9 provides accurate results and is recommended for practical use.
4. An initial free-gas void fraction $\alpha_0 \leq 10^{-7}$ at standard conditions is recommended for use in the proposed FVM-DGCM.
5. The proposed second-order FVM-DGCM simulated the three test cases in this paper reasonably well, and the model exhibited fairly accurate and robust behavior for Courant numbers less than or equal to 1, even when fine computational grids were used.
6. The first-order FVM-DGCM can reach the same accuracy as the second-order FVM-DGCM when $C_r = 1.0$, but it produced strong dissipation for values of $C_r < 1.0$.
7. The FVM-DVCM produced the same results as FVM-DGCM with $C_{-ap} = 1$, and can be regarded as the limiting case of FVM-DGCM when $C_{-ap} = 1$.
8. Compared with the classical MOC-DGCM, the proposed FVM-DGCM produces more reliable pressure histories when fine grids are used.
9. Some measured high-frequency pressure peaks were not reproduced by either numerical model. This was due to the fact that transient cavitation along the pipeline was not homogeneous and stochastic; however, the measured pressure spikes did not affect the bulk pressure pulses significantly.

Acknowledgments

The authors gratefully acknowledge the financial support for this research from the National Natural Science Foundation of China (Grant Nos. 51679066 and 51209073), the Fundamental Research Funds for the Central Universities (Grant No. 2015B15414), the Open Research Fund Program of State Key Laboratory of Water Resources and Hydropower Engineering Science (Grant No. 2016SDG01), and the China Scholarship Council (Grant No. 201606710077).

Notation

The following symbols are used in this paper:

$\boldsymbol{A}, \overline{\boldsymbol{A}}$ = coefficient matrix and linearized coefficient matrix, respectively;
a = wave speed;
C_{-ap} = coefficient of pressure adjustment ranging from 0 to 1;
C_r = Courant number;
D = pipe diameter;
f = Darcy–Weisbach friction factor;
$\mathbf{f}$ = flux term;
g = gravitational acceleration;
H = hydraulic-grade line, also called piezometric head or head;
H_b = absolute barometric pressure head;
$H^n_{g(j)}$ = piezometric head of gas cavity within jth reach at time $n\Delta t$;
H_L, H_R = piezometric head to left and right of interface, respectively;
H_r = upstream reservoir pressure head;
H^n_{uj}, H^n_j = piezometric heads upstream and downstream, respectively, of jth reach at time $n\Delta t$;
H_v = gauge vapor pressure head;
I_i = ith cell;
i, j = index for cell and reach, respectively;
L = pipeline length;
M_g = mass of gas;
N, N_s = number of cells, $N = 2N_s$;
n = index for time t;
p^*_g = absolute pressure of free gas;
p^*_v = absolute vapor pressure;
p^*_0 = absolute standard atmospheric pressure;
Q, Q_u = flow rates in downstream and upstream of gas cavity, respectively;
Q^n_{uj}, Q^n_j = flow rates upstream and downstream, respectively, of jth reach at time $n\Delta t$;
R_g = specific gas constant;
$\mathbf{s}$ = source term;
T = absolute temperature of free gas;
T_c = effective closing time of valve;
t = time;
$\mathbf{U}$ = cell mean value of $\mathbf{u}$;
$\overline{\mathbf{U}}$, $\overline{\overline{\mathbf{U}}}$ = intermediate flow variables in Runge–Kutta scheme;
$\mathbf{U}^n_L$, $\mathbf{U}^n_R$ = average cell value of $\mathbf{u}$ to left and right of interface at time $n\Delta t$;
$\mathbf{u}$ = flow variables H and V;
V = average cross-sectional velocity;
V_L, V_R = average cell velocity to left and right of interface, respectively;
V_0 = initial steady pipe flow velocity;
x = distance along pipeline;
z = pipeline elevation;
α = gas void fraction in control volume;

α_0 = gas void fraction at standard conditions;
Δt = time increment;
Δx, $\Delta x'$ = reach length, $\Delta x' = 2\Delta x$;
$\Delta \forall_{g(j)}$ = volume change of gas cavity;
$\overline{\lambda}_i$ = eigenvalues of $\overline{\boldsymbol{A}}$;
ρ_l = density of liquid;
$\forall$, $\forall_g$ = volume of pipe reach and gas cavity volume, respectively;
$\forall_{g0}$ = initial volume of lumped gas cavity; and
$\forall^n_{g(j)}$ = gas cavity volume in jth reach at time $n\Delta t$.

References

Adamkowski, A., and Lewandowski, M. (2015). "Cavitation characteristics of shut-off valves in numerica1 modelling of transients in pipelines with column separation." *J. Hydraul. Eng.*, 10.1061/(ASCE)HY.1943-7900.0000971, 04014077.

Bergant, A., Karadžić, U., Vítkovský, J., Vušanović, I., and Simpson, A. R. (2005). "A discrete gas-cavity model that considers the frictional effects of unsteady pipe flow." *Strojniški vestnik J. Mech. Eng.*, 51(11), 692–710.

Bergant, A., and Simpson, A. R. (1999). "Pipeline column separation flow regimes." *J. Hydraul. Eng.*, 10.1061/(ASCE)0733-9429(1999)125:8(835), 835–848.

Bergant, A., Simpson, A. R., and Tijsseling, A. S. (2006). "Water hammer with column separation: A historical review." *J Fluid Struct.*, 22(2), 135–171.

Guinot, V. (2000). "Riemann solvers for water hammer simulations by Godunov method." *Int. J. Numer. Meth. Eng.*, 49(7), 851–870.

Liou, J. C. P. (2000). "Numerical properties of the discrete gas cavity model for transients." *J. Fluids Eng.*, 122(3), 636–639.

Malekpour, A., and Karney, B. (2014). "Column separation and rejoinder during rapid pipeline filling induced by a partial flow blockage." *J. Hydraul. Res.*, 52(5), 693–704.

Provoost, G., and Wylie, E. B. (1982). "Discrete gas model to represent distributed free gas in liquids." *Proc., 5th Int. Symp. on Water Column Separation*, IAHR, Obernach, Germany, 28–30.

Simpson, A. R. (1986). "Large water hammer pressures due to column separation in sloping pipes." Ph.D. thesis, Univ. of Michigan, Ann Arbor, MI.

Simpson, A. R., and Bergant, A. (1994). "Numerical comparison of pipe-column-separation models." *J. Hydraul. Eng.*, 10.1061/(ASCE)0733-9429(1994)120:3(361), 361–377.

Toro, E. F. (2009). *Riemann solvers and numerical methods for fluid dynamics: A practical introduction*, 3rd Ed., Springer, Berlin.

Vasconcelos, J. G., and Marwell, D. T. (2011). "Innovative simulation of unsteady low-pressure flows in water mains." *J. Hydraul. Eng.*, 10.1061/(ASCE)HY.1943-7900.0000440, 1490–1499.

Wang, H., et al. (2016). "CFD approach for column separation in water pipelines." *J. Hydraul. Eng.*, 10.1061/(ASCE)HY.1943-7900.0001171, 04016036.

Wylie, E. B. (1984). "Simulation of vaporous and gaseous cavitation." *J. Fluids Eng.*, 106(3), 307–311.

Wylie, E. B., Streeter, V. L., and Suo, L. (1993). *Fluid transients in systems*, Prentice Hall, Englewood Cliffs, NJ.

Zhao, M., and Ghidaoui, M. (2004). "Godunov-type solutions for water hammer flows." *J. Hydraul. Eng.*, 10.1061/(ASCE)0733-9429(2004)130:4(341), 341–348.

Zhou, L., Wang, H., Liu, D. Y., Ma, J. J., Wang, P., and Xia, L. (2017). "A second-order finite volume method for pipe flow with water column separation." *J. Hydro-Environ. Res.*, 17, 47–55.